Available online at www.sciencedirect.com
ScienceDirect
Journal of Sound and Vibration 323 (2009) 677–696
JOURNAL OF SOUND AND VIBRATION
www.elsevier.com/locate/jsvi

A theoretical and experimental investigation of modulation sidebands of planetary gear sets

M. Inalpolat, A. Kahraman*

Department of Mechanical Engineering, The Ohio State University, 201 West 19th Avenue, Columbus, OH 43210, USA

Received 10 July 2008; received in revised form 17 November 2008; accepted 8 January 2009
Handling Editor: S. Bolton
Available online 13 February 2009

Abstract

In this paper, a simplified mathematical model is proposed to describe the mechanisms leading to modulation sidebands of planetary gear sets. The model includes key system parameters such as number of planets, planet position angles, and planet phasing relationships defined by the position angles and the number of teeth of the gears. The model is used to simulate a wide range of gear sets to show that they can be classified in five distinct groups based on their sideband behavior in terms of their frequencies and amplitudes. A special experimental planetary gear set-up is developed and planetary gear sets from of three of these five groups are procured. A methodology is developed to demonstrate modulation sidebands from the ring (internal) gear radial acceleration measurements. For each case, sets of ring gear acceleration measurements at various speed and torque conditions are presented to demonstrate rich sideband activity that agrees well with the model predictions. At the end, based on results of the parametric studies and experiments, general rules on modulation sidebands of planetary gear sets are proposed.

1. Introduction

Planetary gear sets are commonly used in many automotive, aerospace and industrial gearbox applications. As they employ N number of identical planet branches, they allow the power transmitted to be split into N parallel paths to achieve maximum power density (power to weight ratio). In addition, different input-to-output speed (torque) ratios can be achieved with the same planetary gear set by simply changing the input, output and reaction (fixed) members. This feature makes them desirable for several applications such as automotive automatic transmissions. They are also typically quieter than their fixed-center, lay-shaft counterparts as the self-centering capability of central members provide more tolerance to manufacturing errors associated with gears and the carrier.

With these proven advantages in place, planetary gear sets are also known to exhibit several unique behaviors, which cannot be found in other fixed-center gear trains. Some of these behavior such as planet load sharing as a function of manufacturing errors [1,2] and planet mesh phasing for cancellation or neutralization

*Corresponding author. Tel.: +1 614 292 4678.
E-mail address: kahraman.1@osu.edu (A. Kahraman).

0022-460X/$ - see front matter © 2009 Elsevier Ltd. All rights reserved.
doi:10.1016/j.jsv.2009.01.004

of the gear mesh excitations [3,4] have been studied extensively. On the other hand, another unique behavior that most measured vibration and noise data from planetary gear transmissions exhibit, namely modulation sidebands, needs to be studied in a more general and systematic way. They can be recognized as harmonic orders other than the pure tones defined by the gear mesh harmonics in vibration and noise spectra of geared systems. This paper focuses on a detailed investigation the mechanisms of these *sideband* harmonics that appear in the vicinity of the gear mesh harmonic orders at the gear mesh frequency and its integer multiples.

Fig. 1 illustrates a simple planetary gear set that is formed by a sun gear (s), an internal or ring gear (r) and N number of identical planet gears (pinions) located around the sun gear at angles ψ_i ($i \in [1, N]$). In this example, $N = 4$. The planets are held by a common rigid structure, called planet carrier (c) through planet bearings. In this arrangement, planets act as idler gears with no connections to the outside structures of the gearbox, while the central members s, r, and c are either connected to input or output, or fixed with respect to transmission housing. In cases when the sun or ring gear is fixed (stationary), the carrier must rotate with its planets. For instance, in Fig. 1, the ring gear is fixed and a transducer mounted on it or on the housing near the ring gear–housing interface experiences a periodic variation in vibration amplitudes as planets pass through this fixed transducer location. This is known to cause an amplitude modulation (AM) of vibration and noise time histories to result in modulation sidebands in the frequency domain. This is one of the main mechanisms causing planetary gear sidebands.

In addition to sidebands caused by a rotating carrier, a large number of gear manufacturing errors can also cause variations to modulate the dynamic gear mesh forces in three different forms of wave modulations, namely AM, frequency modulations (FM), and phase modulations (PM). These types of modulations were reported to occur frequently in mechanical systems [5,6]. Typical errors of a planetary gear set that might cause modulations include eccentricities and run-out errors of the gears and the carrier, and tooth-to-tooth spacing, tooth thickness and indexing errors [1]. There are other variations due to relative motion of the rotating components of the gear set with respect to the other components that might result in sidebands as well. Among them, radial floating motion of central members such as the sun gear induces instantaneous center distance variations and modulates the gear mesh forces [7]. Likewise, changes in deformations of the components with planet pass, tooth pass or ring gear spline pass as observed from the gears might provide additional mechanisms for sidebands. Finally, the planet load sharing characteristics impact the AM as well as dynamic gear mesh forces, potentially influencing the sidebands of planetary gear sets.

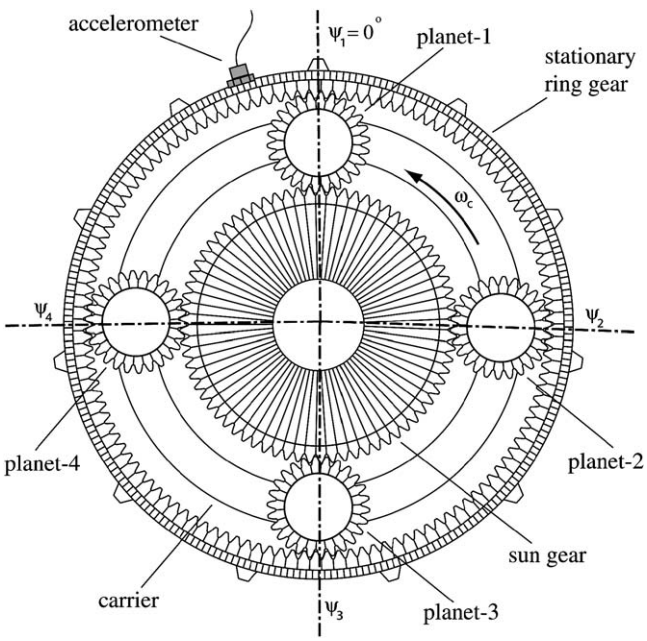

Fig. 1. A schematic showing the components of a 4-planet planetary gear set and an accelerometer mounted on the ring gear.

There are only a few published studies on planetary gear sidebands with significant contributions to the understanding to this subject matter. In one such study, McFadden and Smith [8] predicted the vibration produced at a fixed transducer location on the ring gear of a simple planetary gear set. Their study was the first to explain the underlying reasons for the asymmetric distribution of the modulation sidebands about the tooth meshing frequency. Their model was able to predict the frequency content of the dominant vibration peaks of an example planetary gear set, but not the relative amplitude content. McFadden [9] also developed a technique to calculate the time domain averages of the tooth meshing vibration of the individual planet gears and the sun gear in an epicyclic gearbox. Later, McNames [10] employed continuous-time Fourier series to explore the relative amplitudes of the dominant peaks that can possibly show up in the spectra along with their corresponding frequencies. His model is based on time-domain model of McFadden and Smith [8], with the discrete Fourier series analysis included. McNames reported that the total vibration spectra (sum of the vibrations from each individual planet gear as they pass through a fixed transducer location) will have dominant components only at frequencies that are integer multiples of number of planets in the system. This conclusion was presented for a class of planetary gear sets (equally spaced planets with sequential planet mesh phasing) and its validity was not tested for other planetary gear sets. Besides these two studies, there are a variety of works that deal with sidebands in the wider context of planetary gear vibrations [11–19]. The same is true for studies on planetary vibration condition monitoring for diagnostics purposes [19–23]. While providing a reasonable foundation for amplitude modulated sidebands of planetary gear sets, above studies fall short of providing a general formulation that can be used to classify planetary gear sets based on their sideband behavior and describe the sideband behavior of any arbitrary planetary gear set. Also missing from the literature, besides very limited data provided in Refs. [8,10] from actual field tests of planetary transmissions, is a detailed and dedicated experimental study of modulation sidebands of planetary gear sets for validation of any of these models.

Accordingly, this study first focuses on developing a simplified analytical model to describe AM of planetary gear sets. This model is intended to be general so that any simple planetary gear set having any planet spacing condition (equally or unequally spaced), any number of planets, any number of gear teeth as well as any planet mesh phasing condition (in-phase, sequentially phased or arbitrarily phased) can be analyzed. The model will be used to show that there are various classes of planetary gear sets that exhibit different sideband behavior. Trends observed from each class of gear set will be documented. The second objective of this study is to demonstrate the validity of these trends through an experimental study. For this purpose, an experimental set-up and measurement system will be developed to perform sideband measurements by using gear sets that are qualitatively different in terms of their predicted sideband outcome. At the end, these measured acceleration frequency spectra will be compared to the predictions to assess the fidelity of the proposed analytical model.

2. Analytical model

For a planetary gear set with N planets, consider the kinematic configuration when the sun gear s and the planet carrier c act as the input and output members and the ring gear r is held stationary (its rotational velocity $\omega_r = 0$). In this kinematic configuration, the fundamental gear mesh (tooth passing) frequency is defined as

$$\omega_m = Z_r \omega_c, \tag{1}$$

where ω_c is the absolute angular velocity of the planet carrier and Z_r the number of teeth of the ring gear. In case of the fixed sun gear, Z_r is replaced by the number of teeth of the sun gear Z_s. The planets are positioned at angles ψ_i ($i \in [1, N]$) within the planet carrier. Setting $\psi_1 = 0$ without any loss of generality, other planets can be assembled in any set of discrete angles as long as they are integer multiples of the least mesh angle which can be defined as

$$\lambda = \frac{2\pi}{Z_s + Z_r}. \tag{2}$$

Planet i cannot be assembled at a position angle unless $\psi_i = m\lambda$ (m: integer). Further, a gear set with equally spaced planets at planet position angles $\psi_i = 2\pi(i-1)/N$ is possible only if $(Z_s + Z_r)/N =$ integer. For instance, for a gear pair with $Z_r = 125$ and $Z_s = 73$, $\lambda = 1.8182^\circ$ and a 3-planet carrier can be assembled in equal spacing ($(Z_s + Z_r)/N = \frac{1}{3}(73 + 125) = 66 =$ integer) while equally spaced 4- and 5-planet carriers cannot be assembled with these gears ($\frac{1}{4}(73 + 125) = 49.5$ and $\frac{1}{5}(73 + 125) = 39.6$).

Here, each mesh of the ring gear with each planet i transmits a static (mean) mesh force $\bar{F}_i$ as well as a dynamic force $F_i(t)$ about $\bar{F}_i$ induced by vibratory behavior of the gear pair [4,24]. This dynamic mesh force component is periodic at the gear mesh frequency and can be written in Fourier series for the fixed ring gear case as

$$F_i(t) = \sum_{j=1}^{J} F_{ij} \cos(\mathrm{j} Z_r \omega_c t + \phi_j + \mathrm{j} Z_r \psi_i), \tag{3}$$

where F_{ij} is the Fourier coefficient of j-th harmonic of the dynamic force of ring-planet i mesh, ϕ_j the phase angle of the j-th harmonic component and $Z_r\psi_i$ is the phase angle between the ring gear meshes of planet i and planet 1 [3,4,25].

In Fig. 1, the measured acceleration for the transducer mounted on the outer surface of the ring gear will be modulated as $F_i(t)$ ($i \in [1, N]$) that applies along the line of action of the ring/planet-i mesh rotates with the carrier at a velocity ω_c. For a complete revolution of the carrier, the transducer will experience the disturbances from all N planets in sequence. As the force transmission path between the ring-planet i mesh is rather complex (and can be described quantitatively only by dynamic deformable-body analysis), individual influence of planet-i on the transducer will be assumed to last for a duration of T_c/N where $T_c = 2\pi/\omega_c$ is the rotational period of the carrier. With this assumption, as planet i approaches to the transducer location, its influence will increase for the first $T_c/2N$ time period, reaching its maximum when planet i is at the transducer location and the diminishing to zero at the end of the next $T_c/2N$ time period. This will be followed by planet $(i+1)$ that is assumed to dominate the response of the transducer for the next T_c/N time period, and so on. We conveniently use a Hanning function to represent this phenomenon:

$$w(t) = \frac{1}{2} - \frac{1}{2}\left[\cos\left(\frac{2\pi N t}{T_c}\right)\right]. \tag{4a}$$

With this, for a planet positioned at angle ψ_i, a weighting function is defined as

$$w_i(t) = W_i w\left(t - \frac{\psi_i}{2\pi} T_c\right) U_i(t), \tag{4b}$$

where $U_i(t)$ is defined as

$$U_i(t) = \sum_{n=1}^{\infty}\left\{u\left[t - \left(\frac{(n-1)N + i - 1}{N}\right)T_c\right] - u\left[t - \left(\frac{(n-1)N + i}{N}\right)T_c\right]\right\}. \tag{4c}$$

In this equation, terms $u(t-a)$ are unit step functions ($u(t-a) = 1$ for $t > a$ and $u(t-a) = 0$ for $t < a$) that ensure the influence of planet i on the transducer lasts only for a period of T_c/N. The summation over n is needed to maintain the same periodicity for each carrier rotation. In Eq. (4b), the multiplier $W_i = N\bar{F}_i/\sum_{j=1}^{N}\bar{F}_j$ is intended to account for any unequal load sharing amongst the planets due to the carrier and gear manufacturing errors [1,2]. If all $\bar{F}_i$ are the same (i.e. perfect load sharing), then all $W_i = 1$ in addition to having identical Fourier harmonic amplitudes F_{ij} for $i \in [1, N]$ in Eq. (3). However, if all the N planets do not carry equal share of the load, then $\bar{F}_i$ (and W_i) will be different in addition to F_{ij} that must be determined at this $\bar{F}_i$ value [24].

Eq. (4) represents a major simplification employed by the model. The assumption that the influence of planet i on the transducer lasts only for a period of T_c/N might not be true for certain systems, especially if the ring gear is very flexible. The same formulation can easily be modified to increase the duration in which a planet is effective. The weighting function $w(t)$ defined in Eq. (4a) was also chosen rather arbitrarily to represent the continuously increasing and then diminishing effect of a planet mesh on the observed vibration amplitude. A more accurate and realistic shape for $w(t)$ should be specific to each gear set considered,

depending on its size, ring gear–housing interface and ring gear flexibility. A proper accounting of these effects would require a deformable-body dynamic model that can represent the transfer path between a given gear mesh and the point of measurement accurately.

The acceleration signal caused by dynamic force $F_i(t)$ of the ring/planet-i mesh is assumed to be proportional to the product of $w_i(t)$ and $F_i(t)$ so that

$$a_i(t) = Cw_i(t)F_i(t) = \bar{W}_i w\left(t - \frac{\psi_i}{2\pi}T_c\right) U_i(t) \sum_{j=1}^{J} F_{ij} \cos(\mathrm{j}Z_r\omega_c t + \phi_j + \mathrm{j}Z_r\psi_i), \tag{5a}$$

where $\bar{W}_i = CW_i$ and C is a constant. Fig. 2 illustrates $F_i(t)$, $w_i(t)$ and the total acceleration signal $a(t)$ that is given as

$$a(t) = \sum_{i=1}^{N} a_i(t) \tag{5b}$$

for a 3-planet ($N = 3$) gear set having equal spacing ($\psi_1 = 0$, $\psi_2 = 2\pi/3$ and $\psi_3 = 4\pi/3$), assuming harmonic $F_i(t)$ ($J = 1$ in Eq. (5a)) with $\bar{W}_i = 1$ and $Z_r = 25$. Since the overall time signal $a(t)$ shown in Fig. 2 is heavily modulated, the corresponding frequency spectrum

$$A(\omega) = \int_{-\infty}^{\infty} |a(t)\mathrm{e}^{-\mathrm{i}\omega t}|\,\mathrm{d}t \tag{6}$$

would reveal significant sideband activity around the gear mesh harmonic frequency $\omega_m = Z_r\omega_c$.

Eq. (5a) should work for planetary gear sets that act in a linear time-varying fashion as it is the case for most planetary gear sets formed by helical gears. The time-varying coefficients are due to periodic fluctuations of the gear mesh stiffnesses that act as parametric excitations for the predicted periodic dynamic gear mesh forces $F_i(t)$ [24,26]. In spur planetary gear sets, however, it is possible to have nonlinear behavior within the primary and parametric resonance regimes [26] limiting the use of Eq. (5a) at operating speeds within the off-resonance regions.

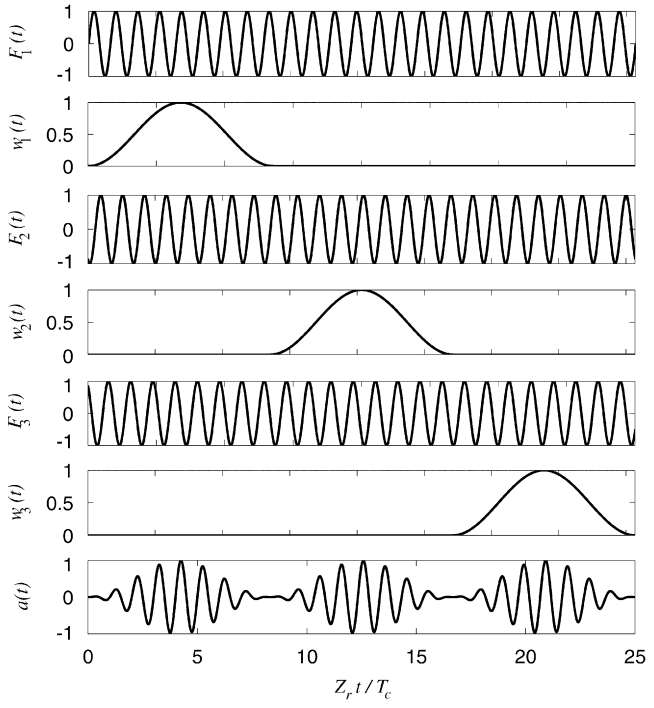

Fig. 2. A schematic illustration of $F_i(t)$, $w_i(t)$ and $a(t)$ for a gear set having $N = 3$ and $Z_r = 25$.

In the presence of manufacturing errors that are periodic over a complete carrier (ring gear) revolution as described in Section 1, one would be required to define another function in the form

$$R(\theta) = \bar{R} + \sum_{k=1}^{K} R_k \sin(k\theta + \phi_k), \tag{7}$$

where, $\bar{R}$ is the average over complete rotation. Here, k is the harmonic index, and R_k and ϕ_k are the amplitude and the phase angle of that particular Fourier component. Each planet i is subjected to this variation with $\theta_i = \omega_c t + \psi_i$ so that

$$R_i(t) = \bar{R} + \sum_{k=1}^{K} R_k \sin(k\omega_c t + k\psi_i + \phi_k). \tag{8}$$

With this additional variation,

$$a_i(t) = w_i(t) F_i(t) R_i(t) \tag{9}$$

and Eq. (5b) is still valid, now with this form of $a_i(t)$. Similar variations can be introduced at the sun gear rotational frequency to account for the errors associated with it, while they should be less important as path between each sun mesh and the transducer is longer and sun is commonly allowed to float radially to compensate for some of these errors.

Assuming that $R_i(t) = \bar{R}$, Eq. (5) indicates that there are $N+2$ main parameters (N, Z_r, ψ_1, $\psi_2, \ldots, \psi_N$) dictating any sideband activity observed in frequency domain. With the restrictions induced by Eq. (2) in terms of where planets can be positioned for suitable assembly conditions, five different conditions are possible, each causing a different form of modulation sidebands.

Case (i): *Equally spaced planets and in-phase gear meshes*. This condition is defined mathematically as

$$\psi_i = \frac{2\pi(i-1)}{N} \quad \text{and} \quad \frac{Z_r \psi_i}{2\pi} = n \quad (n: \text{ integer}). \tag{10}$$

The first condition indicates that the planets are equally spaced while the second condition ensures all $F_i(t)$ in Eq. (3) are in phase. For this case with equally spaced planets, a simpler form of the second condition is that Z_r must divisible by N (i.e. $Z_r/N =$ integer) for all ring gear meshes to be in phase. Assuming equal load sharing ($W_i = 1$, $F_{ij} = F_j$, $i \in [1,N]$) and considering a single harmonic term ($J = 1$) in Eq. (3) as the mesh forces that are in phase, $F_i(t) = F(t) = F_1 \cos Z_r \omega_c t$, further ignoring the once-per revolution errors in Eq. (8), Eq. (5b) is written as

$$a(t) = F(t) \sum_{i=1}^{N} w_i(t) = F(t) \sum_{i=1}^{N} w\left(t - \frac{\psi_i}{2\pi} T_c\right) U_i(t). \tag{11a}$$

Under the conditions assumed in this case, $w(t)$ becomes periodic at T_c/N, reducing Eq. (11a) to

$$a(t) = CF(t) w(t) = CF_1 \cos(Z_r \omega_c t)[\tfrac{1}{2} - \tfrac{1}{2}\cos(N\omega_c t)], \tag{11b}$$

which can be written as

$$a(t) = CF_1\{\tfrac{1}{2}\cos(Z_r\omega_c t) - \tfrac{1}{4}\cos[(Z_r + N)\omega_c t] - \tfrac{1}{4}\cos[(Z_r - N)\omega_c t]\}. \tag{11c}$$

This indicates that the corresponding frequency spectrum will have gear mesh component at frequency $Z_r\omega_c$ and two symmetric sidebands at half-amplitude as the mesh harmonic at frequencies $(Z_r + N)\omega_c$ and $(Z_r - N)\omega_c$.

Fig. 3 illustrates $A(\omega)$ spectra (with $CF_1 = 1$) for four different planetary gear sets, satisfying conditions given in Eq. (10). The first gear set represented by Fig. 3(a) has $N = 3$ with $Z_r = 123$ and $Z_s = 72$. The second gear set in Fig. 3(b) is a 4-planet system ($N = 4$) with $Z_r = 124$ and $Z_s = 72$, while a 5-planet gear set with $Z_r = 125$ and $Z_s = 70$ is represented by the spectrum of Fig. 3(c). Finally, a gear set having $N = 6$, $Z_r = 126$ and $Z_s = 72$ results in the spectrum shown in Fig. 3(d). All four spectra correspond to Eq. (11c).

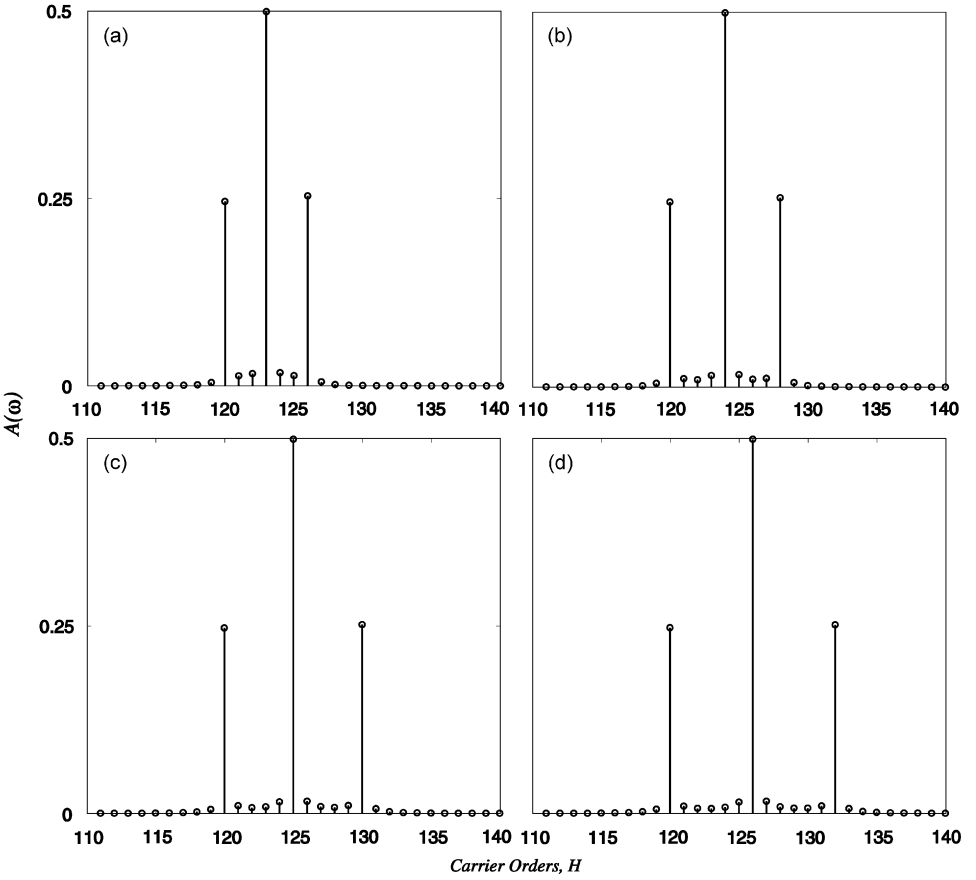

Fig. 3. Theoretical $A(\omega)$ spectra for four different in-phase and equally spaced planetary gear sets: (a) $N=3$, $Z_r=123$ and $Z_s=72$, (b) $N=4$, $Z_r=124$ and $Z_s=72$, (c) $N=5$, $Z_r=125$ and $Z_s=70$, and (d) $N=6$, $Z_r=126$ and $Z_s=72$.

It can be concluded from the formulation presented above and Fig. 3 that this case exhibits the largest harmonic amplitude $A_m=A_{\max}$ at the gear mesh order ($H_m=\omega_m/\omega_c=Z_r$). Two sideband orders of $H=(\omega_m\pm N\omega_c)/\omega_c=H_m\pm N$ and equal amplitude $\frac{1}{2}A_m$ are the only significant sidebands in this case.

Case (ii): *Equally spaced planets and sequentially phased gear meshes*. This case is defined as

$$\psi_i=\frac{2\pi(i-1)}{N},\quad \frac{Z_r\psi_i}{2\pi}\neq n \quad\text{and}\quad \sum_{i=1}^{N}Z_r\psi_i=m\pi \quad (m,n=\text{integers}). \tag{12}$$

Here, the second condition indicates that the planets are not in phase ($Z_r/N\neq$integer for equally spaced planets). Meanwhile, the third condition states that $F_i(t)$ in Eq. (3) are sequentially phased, i.e. sum of the phase angles is an integer multiple of π. This is indeed one of the most common conditions used in product applications since it was shown to result in lower vibration and noise levels [4,24]. It can also be stated that this is the only other possible phasing condition for equally spaced systems other than in-phase condition.

Figs. 4(a–d) illustrate $A(\omega)$ spectra of four different planetary gear sets (again with $CF_1=1$), respectively, each satisfying conditions defined by Eq. (12): (a) $N=3$, $Z_r=125$ and $Z_s=73$, (b) $N=4$, $Z_r=126$ and $Z_s=74$, (c) $N=5$, $Z_r=126$ and $Z_s=74$, and (d) $N=6$, $Z_r=122$ and $Z_s=70$. For instance, for gear set (a), $Z_r/3=125/3=41.\bar{6}$, $Z_r\psi_1=0$, $Z_r\psi_2=(125)\frac{2\pi}{3}\equiv\frac{4\pi}{3}$ and $Z_r\psi_3=(125)\frac{4\pi}{3}\equiv\frac{2\pi}{3}$ such that the third condition in Eq. (12) is also satisfied, i.e. $\sum_{i=1}^{3}Z_r\psi_i=0+\frac{4\pi}{3}+\frac{2\pi}{3}=2\pi$.

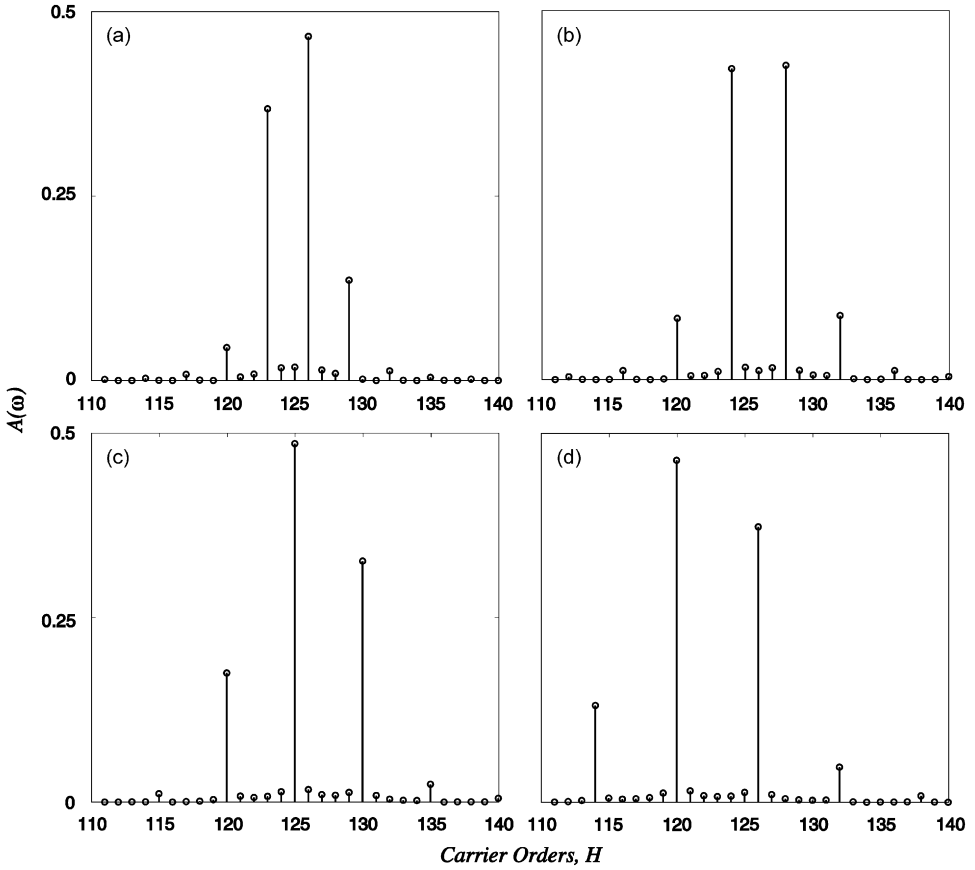

Fig. 4. Theoretical $A(\omega)$ spectra for four different sequentially phased and equally spaced planetary gear sets: (a) $N=3$, $Z_r=125$ and $Z_s=73$, (b) $N=4$, $Z_r=126$ and $Z_s=74$, (c) $N=5$, $Z_r=126$ and $Z_s=74$, and (d) $N=6$, $Z_r=122$ and $Z_s=70$.

In this case, it is not possible mathematically to reduce $a(t)$ to a sum of harmonic terms as it was done for Case (i) since each T_c/N time segment associated with each planet has a different phase angle. Yet, the behavior presented by Fig. 4 has several well-defined traits:

(1) In direct contrast to Case (i), gear sets in this group exhibit nearly zero amplitude ($A_m \approx 0$) at the mesh harmonic order H_m. This is evident from all four cases considered in Fig. 4.
(2) All significant harmonic orders with sizable amplitudes are at orders $H=nN$ (n: integer) in the vicinity of mesh harmonic order H_m, i.e. they all appear at integer multiples of the number of planets N. In Fig. 4(a), for instance, for $N=3$, $Z_r=125$ and $Z_s=73$, there are four harmonics with large amplitudes at orders of 120, 123, 126 and 129, corresponding to $H=40N$, $41N$, $42N$ and $43N$. The same is true for the other three cases as well.
(3) Sidebands are mostly not symmetric about H_m. The harmonic order with the largest amplitude is the order $H=nN$ that is closest to H_m, i.e. $A \approx A_{\max}$ for the order satisfying the condition $|H_{\max}-H_m|<\frac{1}{2}N$. In Fig. 4(a), order $H_{\max}=42N=126$ satisfy this condition, while it is $H_{\max}=25N=125$ for the third example in Fig. 4(c) where $H_m=126$.
(4) A special condition rises when the remainder of the ratio Z_r/N is equal to $\frac{1}{2}$. Even numbers for N and Z_r are necessary (but not sufficient) conditions for this situation. As an example of this, Fig. 4(b) exhibits harmonic orders that are symmetric about H_m and $A \approx A_{\max}$ at two orders where $|H_{\max}-H_m|=\frac{1}{2}N$.

Planetary gear sets satisfying Case (ii) conditions seems to be the only ones considered in the previous planetary sideband studies including those by McFadden and Smith [8] and McNames [10]. These earlier

studies reported that the dominant harmonic orders in the vicinity of the mesh are distributed apart by N orders at integer multiples of N in agreement with the second observation above.

Case (iii): *Unequally spaced planets and in-phase gear meshes.* This condition satisfies the following:

$$\psi_i \neq \frac{2\pi(i-1)}{N} \quad \text{and} \quad \frac{Z_r\psi_i}{2\pi} = n \quad (n = \text{integers}). \tag{13}$$

Here $F_i(t)$ are in phase in spite of the fact that planet spacing is not equal (but still meets the assembly requirements, i.e. all ψ_i are integer multiples of λ). Four examples meeting these conditions are analyzed in Fig. 5: (a) $N=3$, $Z_r=126$ and $Z_s=72$ with $\psi_i=0$, $\frac{2\pi}{3}$ and $1.\bar{2}\pi$ ($\psi_i=0$, 120° and 220°) where planet-3 moved 20° from its equal spacing position, (b) $N=4$, $Z_r=120$ and $Z_s=72$ with $\psi_i=0$, 0.4167π, π and 1.4167π ($\psi_i=0$, 75°, 180° and 255°) corresponding to an in-phase "X-shaped" arrangement where there are two diametrically opposed planet pairs, (c) $N=5$, $Z_r=145$ and $Z_s=75$ with $\psi_i=0$, 0.4276π, 0.8276π, 1.2π and 1.6π (0, 76.97°, 148.97°, 216° and 288°) where planets 2 and 3 are positioned away from their equal spacing angles, and (4) $N=6$, $Z_r=130$, $Z_s=70$, $\psi_i=0$, 0.4π, 0.74π, π, 1.37π and 1.74π (0, 72°, 133.2°, 180°, 246.6° and 313.2°). All of these cases satisfy conditions given by Eq. (13).

The frequency spectra of gear sets having this design condition have the following common features:

(1) The harmonic order with the largest amplitude is the gear mesh harmonic H_m with $A_{\max}=A_m$ as in Case (i). In all four spectra shown in Fig. 5, order $H=H_m=Z_r$ has $A_{\max}=A_m\approx\frac{1}{2}$.

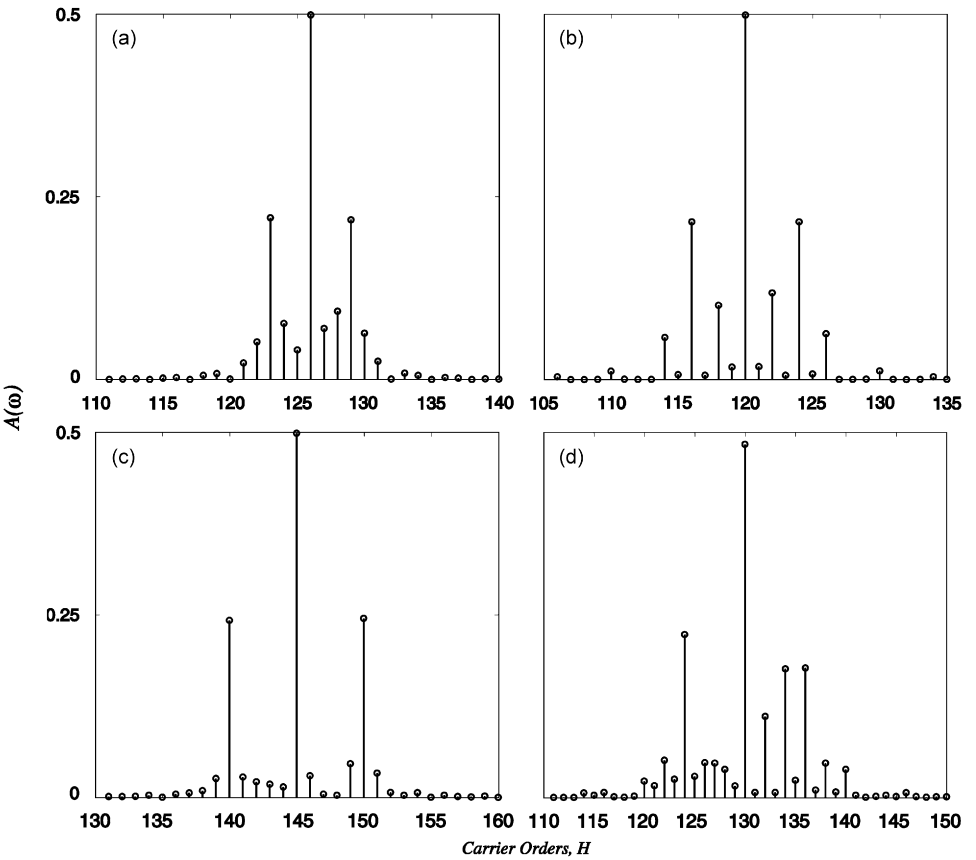

Fig. 5. Theoretical $A(\omega)$ spectra for four different in-phase and unequally spaced planetary gear sets: (a) $N=3$, $Z_r=126$ and $Z_s=72$ with $\psi_i=0$, $\frac{2\pi}{3}$ and $1.\bar{2}\pi$, (b) $N=4$, $Z_r=120$ and $Z_s=72$ with $\psi_i=0$, 0.4167π, π and 1.4167π, (c) $N=5$, $Z_r=145$ and $Z_s=75$ with $\psi_i=0$, 0.4276π, 0.8276π, 1.2π, 1.6π, and (d) $N=6$, $Z_r=130$, $Z_s=70$, $\psi_i=0$, 0.4π, 0.74π, π, 1.37π and 1.74π.

(2) The harmonic orders at $H_m \pm N$ are always the most significant sidebands that are nearly symmetric about H_m. For instance, orders 140 and 150 in Fig. 5(c) are such sidebands that are symmetric about the mesh order $H_m = 145$.
(3) If both N and Z_r are even numbers, then several even orders at $H_m \pm 2n$ dominate the spectrum as shown in Figs. 5(b) and (d). On the other hand, if N is odd, then sidebands appear at many of orders $H_m \pm n$, as in Figs. 5(a) and (c).
(4) As a special condition for this case, if the planets are positioned in diametrically opposed pairs ($N =$ even and the spacing between each planet in the pair is 180°), then the sideband orders exist at even multiples of the carrier order at orders $H_m \pm 2n$ (n: integer), as it the case in Fig. 5(b).

Case (iv): *Unequally spaced planets and sequentially phased gear meshes*. This case is defined by

$$\psi_i \neq \frac{2\pi(i-1)}{N}, \quad \frac{Z_r \psi_i}{2\pi} \neq n \quad \text{and} \quad \sum_{i=1}^{N} Z_r \psi_i = m\pi \quad (m, n = \text{integers}). \tag{14}$$

$A(\omega)$ spectra for four different examples of this case are shown in Fig. 6. Fig. 6(a) is for a system having $N = 3$, $Z_r = 125$, $Z_s = 73$, $\psi_i = 0, 0.\bar{5}\pi$ and $1.\bar{4}\pi$ ($\psi_i = 0$, 100° and 260°). Second example is a 5-planet gear set with $Z_r = 125$, $Z_s = 73$, $\psi_i = 0$, 0.404π, 0.798π, 1.202π and 1.596π ($\psi_i = 0$, 72.727°, 143.636°, 216.364° and 287.273°) and has the spectra shown in Fig. 6(b). Third example is a 4-planet gear set with $Z_r = 126$, $Z_s = 74$, and $\psi_i = 0$, 0.54π, 0.97π, and 1.57π ($\psi_i = 0$, 97.2°, 174.6°, 282.6°) whose predicted spectrum is shown in Fig. 6(c).

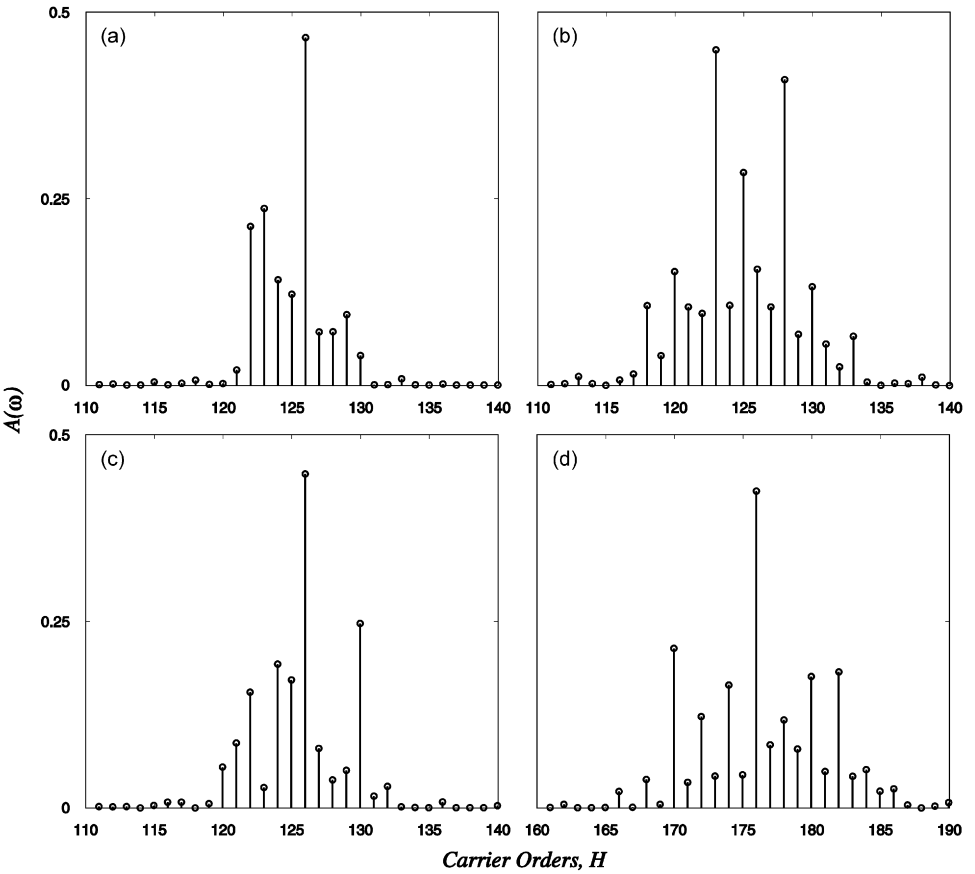

Fig. 6. Theoretical $A(\omega)$ spectra for four different sequentially phased and unequally spaced planetary gear sets: (a) $N = 3$, $Z_r = 125$, $Z_s = 73$, $\psi_i = 0$, $0.\bar{5}\pi$ and $1.\bar{4}\pi$, (b) $N = 5$, $Z_r = 125$, $Z_s = 73$, $\psi_i = 0$, 0.404π, 0.798π, 1.202π and 1.596π, (c) $N = 4$, $Z_r = 126$, $Z_s = 74$, and $\psi_i = 0$, 0.54π, 0.97π, and 1.57π, and (d) $N = 6$, $Z_r = 176$, $Z_s = 74$, and $\psi_i = 0$, 0.376π, 0.704π, π, 1.376π and 1.68π.

The last example represented in Fig. 6(d) is a 6-planet gear set with $Z_r = 176$, $Z_s = 74$, and $\psi_i = 0,\ 0.376\pi,\ 0.704\pi,\ \pi,\ 1.376\pi$ and 1.68π ($\psi_i = 0,\ 67.68^\circ,\ 126.72^\circ,\ 180^\circ,\ 247.68^\circ,\ 302.4^\circ$) .

The spectra corresponding to such gear sets are more complex, with the following common features:

(1) In general, sideband harmonics appear at several integer multiples of the carrier order at $H_m \pm n$ (n: integer) in an asymmetric way around H_m. The number of sidebands with non-zero amplitudes is quite high in each case considered in Fig. 6. For instance, there are about 15 sidebands with sizable amplitude in the spectrum of the third gear set.
(2) In regards to the mesh harmonic order, $A_{\max} = A_m$ when both Z_r and N are even numbers, as exemplified by Figs. 6(c) and (d) where $H_{\max} = H_m = Z_r$. For such systems, if there is at least one diametrically opposed planet pair, then the sidebands at even numbered orders are dominant.
(3) If both Z_r and N are odd numbers, then the gear mesh harmonic order, while non-zero, does not represent the largest amplitude.

Case (v): *Unequally spaced planets and arbitrarily phased gear meshes.* The last and perhaps the most arbitrary case is obtained when the planets are positioned unequally at multiples of λ and planet phasing is arbitrary (neither in-phase nor sequentially phased) such that

$$\psi_i \neq \frac{2\pi(i-1)}{N}, \quad \frac{Z_r\psi_i}{2\pi} \neq n \quad \text{and} \quad \sum_{i=1}^{N} Z_r\psi_i \neq m\pi \quad (m, n = \text{integers}). \tag{15}$$

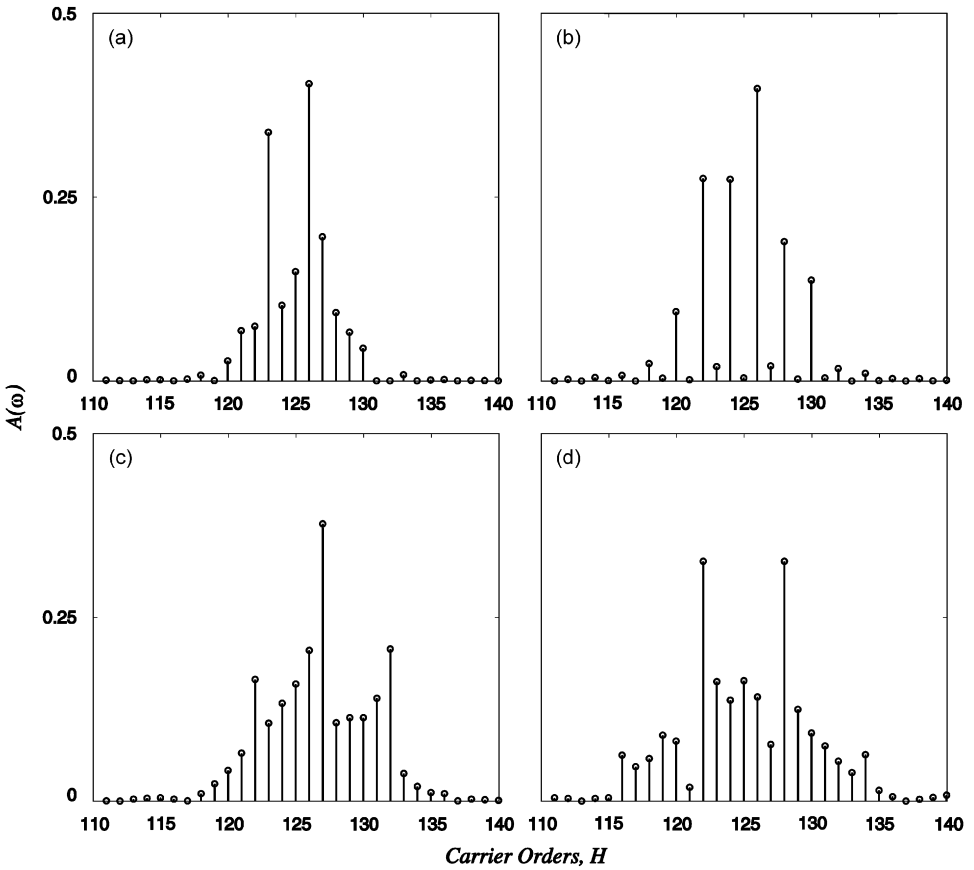

Fig. 7. Theoretical $A(\omega)$ spectra for four different arbitrarily phased and unequally spaced planetary gear sets: (a) $N = 3$, $Z_r = 125$, $Z_s = 73$ and $\psi_i = 0,\ 0.\overline{55}\pi$ and 1.384π, (b) $N = 4$, $Z_r = 125$, $Z_s = 73$ and $\psi_i = 0,\ 0.505\pi,\ \pi$ and 1.505π, (c) $N = 5$, $Z_r = 127$, $Z_s = 73$ and $\psi_i = 0,\ 0.42\pi,\ 0.83\pi,\ 1.24\pi$ and 1.65π, and (d) $N = 6$, $Z_r = 125$, $Z_s = 73$, and $\psi_i = 0,\ 0.\overline{34}\pi,\ 0.\overline{68}\pi,\ 1.\overline{03}\pi,\ 1.\overline{34}\pi,\ 1.\overline{66}\pi$.

Similar to the previous cases, four examples are chosen here to illustrate this case in Fig. 7. The first example is a 3-planet system with $Z_r = 125$, $Z_s = 73$ and $\psi_i = 0,\ 0.\overline{55}\pi$ and 1.384π ($\psi_i = 0,\ 100^\circ$ and 249.13°) and exhibiting a spectrum as shown in Fig. 7(a). The second example is a "X-shaped" 4-planet gear set having $Z_r = 125$, $Z_s = 73$ and $\psi_i = 0,\ 0.505\pi,\ \pi$ and 1.505π ($\psi_i = 0,\ 90.909^\circ,\ 180^\circ$ and 270.909°). In this case, phase angles $Z_r\psi_i = 0,\ 1.1325\pi,\ \pi$ and 0.1312π and the sum of the phase angles is obviously not an integer multiple of π. The corresponding spectrum for this gear set is given in Fig. 7(b). The other example corresponding to the spectrum shown in Fig. 7(c) is a gear set having $N = 5$, $Z_r = 127$, $Z_s = 73$ and $\psi_i = 0,\ 0.42\pi,\ 0.83\pi,\ 1.24\pi$ and 1.65π ($\psi_i = 0,\ 75.6^\circ,\ 149.4^\circ,\ 223.2^\circ$ and 297°). As a last example for this case, a 6-planet gear set is chosen with $Z_r = 125$, $Z_s = 73$, and $\psi_i = 0,\ 0.\overline{34}\pi,\ 0.\overline{68}\pi,\ 1.\overline{03}\pi,\ 1.\overline{34}\pi$, and $1.\overline{66}\pi$ ($0,\ 61.8181^\circ,\ 123.6362^\circ,\ 185.4543^\circ,\ 241.8181^\circ$, and 300°) is chosen. This irregularly-spaced system exhibits a frequency spectrum as shown in Fig. 7(d).

The spectra shown in Fig. 7 illustrate a very rich sideband activity for gear sets satisfying the conditions for this case, with sideband orders at $H_m \pm n$ that are asymmetric about H_m. It is not possible to draw many conclusions from Fig. 7, except to say that even numbered sideband orders are stronger for an even N. Meanwhile, if N is an odd number, then sidebands appear at almost every order neighboring H_m.

3. An experimental study of planetary modulation sidebands

3.1. Experimental test set-up

In order to check the validity of the analytical formulation described in Section 2, a set of tightly controlled planetary gear set experiments were performed. An experimental set-up from a recent study on planet load sharing [1,27] was used with some modifications to study the sidebands of planetary gear sets. We refer to

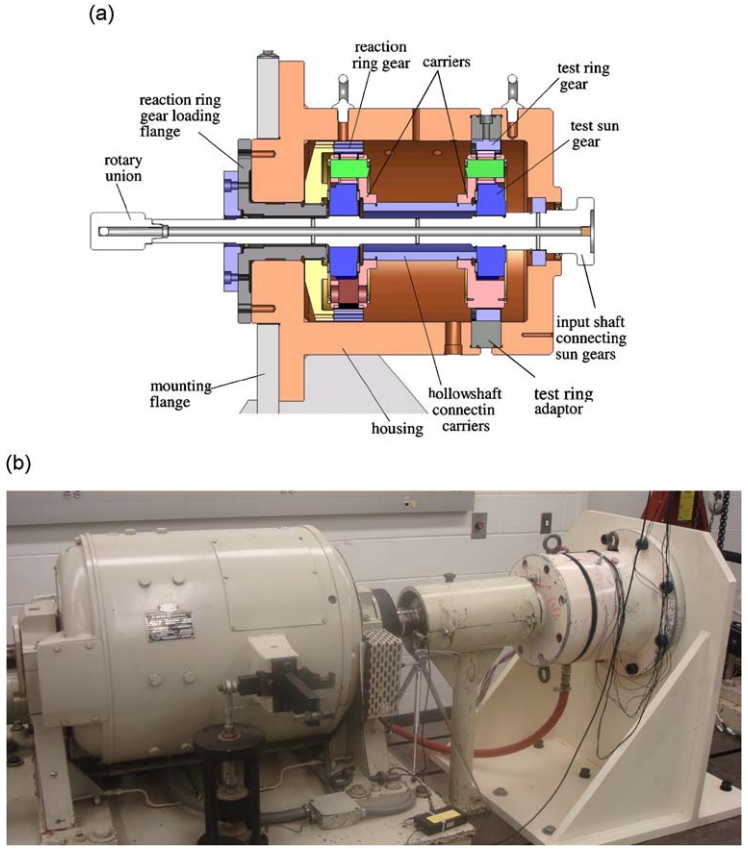

Fig. 8. (a) Cross-section of the back-to-back planetary test fixtures and (b) a view of the test set-up on a transmission dynamometer.

these references in regards to the details of the test set-up and provide here only the aspects that are directly related to this study.

The test set-up uses a "back-to-back" power circulation type arrangement whose cross-section is shown in Fig. 8(a). In this arrangement, the sun gears of two identical planetary gear sets (a test gear set and a reaction gear set) are connected to each other through splines on a common shaft. Likewise, the carrier of the test gear set is connected to the carrier of the reaction gear set via a rigid hollow shaft. The ring gear of the test gear set is held stationary while an external torque is applied mechanically to the ring gear of the reaction gear set forming a closed power loop. In this fixed-ring configuration, a sun gear torque T_s is achieved conveniently by applying a torque of $T_r = Z_r T_s/Z_s$ to the reaction ring gear via a torque arm and calibrated weights. Fig. 8(b) shows a picture of the fixtures mounted on a dynamometer. Here, a DC motor is connected to the shaft of the sun gears to rotate both gear sets while the gear meshes carry the load imposed by the torque trapped in the closed loop through the external torque T_r applied to the reaction ring gear.

3.2. Test gear sets and test matrix

A medium-size planetary gear set design used earlier in Refs. [1,27] was adapted here as the test planetary gear set. All of the gears shown in Fig. 9(a) were hard ground to tight tolerances in order to achieve very accurate profiles while minimizing errors associated with planet tooth thickness and planet pitch line run-out in an attempt to minimize the once-per-revolution errors captured in Eq. (7). The same level of accuracy was applied to the fabrication of the carriers shown in Fig. 9(b) as well, so that an ideal planet load sharing can be achieved [1]. This allows all W_i to be the same ($i \in [1, N]$) in Eq. (4b). Under these conditions, most of the sideband should originate from the kinematic motions of the planet meshes with respect to a fixed transducer location. The test ring gear shown in Fig. 9(a) has a wall thickness of 10.4 mm that is the difference between outside radius and the root circle radius, $R_{\text{out}} - R_{\text{root}}$. With this, the ring gear thickness parameter is calculated as $\Gamma = (R_{\text{out}} - R_{\text{root}})/R_{\text{root}} = 0.083$, that was shown to exhibit limited hoop deflections under load values up to $T_s = 1000$ Nm [28].

The five distinct cases identified in Section 2 would require design and procurement of five different planetary gear sets with appropriate values for the $N+2$ parameters (N, Z_r, $\psi_1, \psi_2, \ldots, \psi_N$) so that each gear

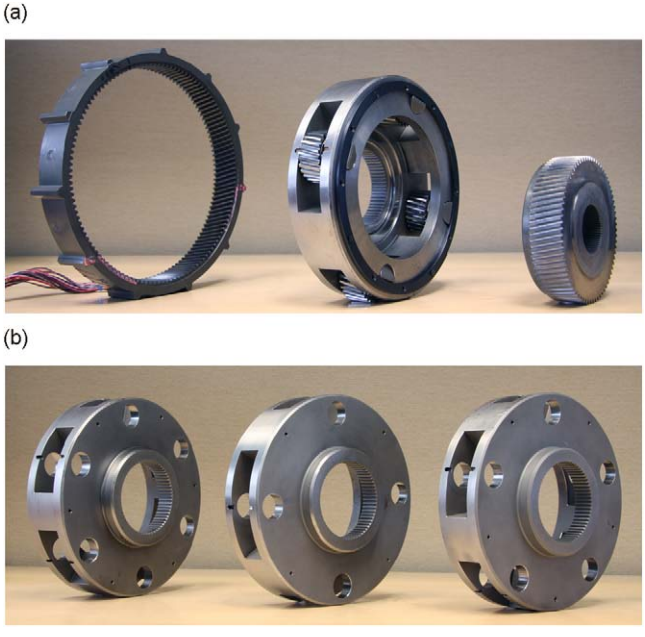

Fig. 9. (a) A set of test gears and (b) 3, 4 and 5 planet carriers used in this study. The 3-planet carrier was designed to accommodate 6 planets as well.

set satisfies the conditions defined by one of the Eqs. (10) and (12)–(15). Since this is very time consuming and costly, this study considered the same baseline gear set design with $Z_s = 73$ and $Z_r = 125$. The remaining parameters $(N, \psi_1, \psi_2, \ldots, \psi_N)$ were varied to obtain three different gear sets, each representing a different case defined in Section 2.

Gear set A. With $Z_s = 73$ and $Z_r = 125$, this 3-planet gear set ($N = 3$) has planets at $\psi_i = 0, \frac{2\pi}{3}, \frac{4\pi}{3}$ since equally spaced planet condition is met, i.e. $(Z_r + Z_s)/N = (73 + 125)/3 = 66 = \text{integer} = 1.8182^\circ$. In addition, planet gear meshes are sequentially phased since $Z_r/3 = 125/3 = 41.\bar{6}$, $Z_r\psi_1 = 0$, $Z_r\psi_2 = (125)\frac{2\pi}{3} \equiv \frac{4\pi}{3}$ and $Z_r\psi_3 = (125)\frac{4\pi}{3} \equiv \frac{2\pi}{3}$. Therefore, Eq. (12) is satisfied and this gear set represents Case (ii) in the previous section in terms of its sideband activity. This gear set is indeed the example gear set (a) for this case whose predicted spectrum is shown in Fig. 4(a).

Gear set B. Again with $Z_s = 73$ and $Z_r = 125$ (the same gears), this 5-planet gear set ($N = 5$) was obtained by designing a 5-planet carrier shown in Fig. 9(b) with planet spacing angles of $\psi_i = 0, 0.404\pi, 0.798\pi, 1.202\pi$ and 1.596π ($\psi_i = 0, 72.727^\circ, 143.636^\circ, 216.364^\circ$ and 287.273°). Here, the equal spacing condition is not satisfied since $(73 + 125)/5 = 39.6$ (not an integer) while assembly condition is met since all ψ_i are integer multiples of the least mesh angle of $\lambda = 1.8182^\circ$. In addition, $\sum_{i=1}^{5} Z_r\psi_i \equiv 0 + 0.505\pi + 1.747\pi + 0.253\pi + 1.495\pi = 4\pi$, indicating that the gear meshes are sequentially phased. Accordingly, this gear set satisfies Eq. (14) and represents an unequally spaced and sequentially phased gear set of Case (iv) type. Fig. 6(b) illustrates the predicted acceleration spectra for this planetary gear set.

Gear set C. The last experimental planetary gear set was obtained with the same gears ($Z_s = 73$ and $Z_r = 125$), and an X-shaped 4-planet carrier ($N = 4$) shown in Fig. 9(b). In this arrangement, the planets are at angles of $\psi_i = 0, 0.505\pi, \pi$ *and* 1.505π ($\psi_i = 0, 90.909^\circ, 180^\circ$ and 270.909°). Here, the planet pairs 1–3 and 2–4 are diametrically opposed while the equal spacing and special (in-phase or sequentially phased) phasing conditions are not met as $Z_r\psi_i = 0, 1.131\pi, \pi, 0.131\pi$. Accordingly, this case represents an unequally spaced and arbitrarily phased gear set of Case (v) type, satisfying the mathematical conditions of Eq. (15). The predicted sideband activity for this gear set was given in Fig. 7(b).

Various tests for each of gear sets A, B and C were performed within the sun gear speed and torque ranges of $\Omega_s = 200{-}3200$ rev/min and $T_s = 200{-}1000$ Nm (corresponding to a reaction ring gear torque range of $T_r = 342$–1712 Nm). Several of these tests were repeated more than once to ensure that the repeatability of the data is maintained throughout the entire test procedure.

3.3. Instrumentation, data collection and data analysis

The ring gear of the test side gear set was held stationary through 11 equally spaced external spline teeth as shown in Fig. 10. Eleven miniature accelerometers (PCB-353B15) were mounted on the ring gear outside

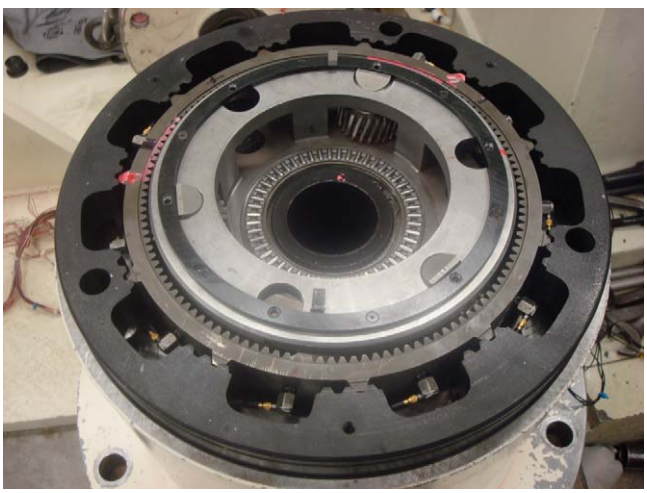

Fig. 10. A view of the accelerometers mounted radially on the outside surface of the test ring gear.

surface radially at an equal spacing of 32.72°. Each accelerometer was at a location representing the mid-point between the adjacent spline teeth. The accelerometer signals were conditioned before being recorded by a 16-channel digital data recorder. The data was processed off-line to obtain the acceleration spectra measured by all 11 transducers. As the sideband activities detected by all accelerometers were nearly identical, data from only one of the accelerometers will be provided in the next section. In addition, a photoelectric sensor was used to generate a once-per-revolution signal of the sun gear shaft. Using the gear reduction ratio, this was scaled to obtain a once-per-revolution signal for the rotation of the carrier, which was analyzed simultaneously with all of the acceleration signals to allow proper averaging of the collected data.

For each particular test, 5 s segments of acceleration time histories were collected together with the sun shaft reference signal. They were next averaged synchronously and a fast Fourier transform (FFT) routine was used to obtain frequency spectra corresponding to each averaged time history. The frequency scales of the resultant spectra were normalized by the carrier rotation frequency to obtain the corresponding order spectra with $H = \omega/\omega_c$.

3.4. Experimental results

Fig. 11 shows example measured $a(t)$ time histories for gear sets A, B and C at certain load and speed conditions. In these figures, the time axis is normalized by the mesh cycle period T_c/Z_r and a data segment covering a complete carrier rotation is presented. In Fig. 11(a) for gear set A ($N = 3$), an apparent AM is observed that repeats three times. Similar modulation patterns are observed in Figs. 11(b) and (c) for gear sets B and C with 4 and 5 planets, respectively. As a result, the FFT spectra $A(\omega)$ of these time histories exhibit significant number of sidebands around the gear mesh harmonic order H_m as well as around the higher gear mesh harmonics ($2H_m$, $3H_m$, $4H_m$ and so on). Fig. 12 illustrates such sidebands on the order spectrum corresponding to the time history given in Fig. 11(a). Here, while the amplitudes are different, the same trends are observed around each mesh harmonic order.

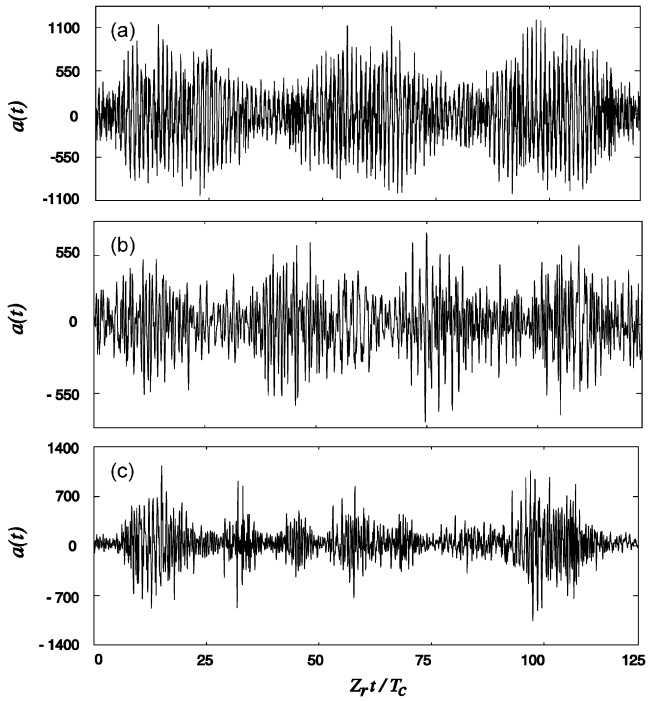

Fig. 11. Examples of measured $a(t)$ in m/s^2 at $\Omega_s = 3200$ rev/min from: (a) gear set A ($N = 3$) at $T_s = 800$ Nm, (b) gear set C ($N = 4$) at $T_s = 1000$ Nm, and (c) gear set B ($N = 5$) at $T_s = 1000$ Nm.

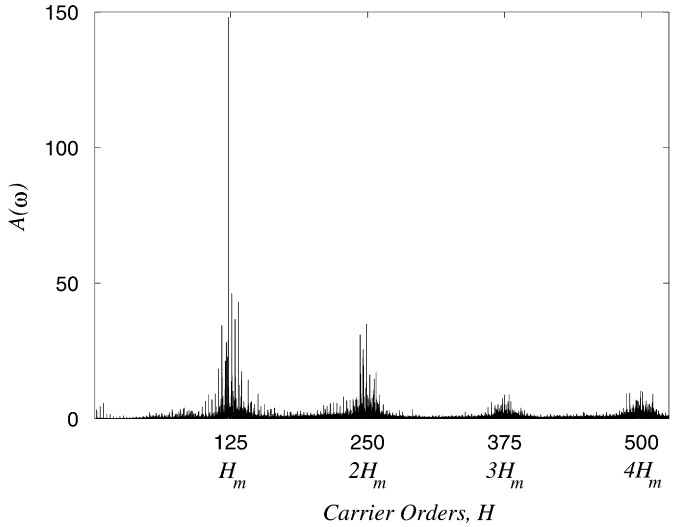

Fig. 12. An example measured acceleration frequency spectrum for the gear set A at $T_s = 800$ Nm and $\Omega_s = 3200$ rev/min.

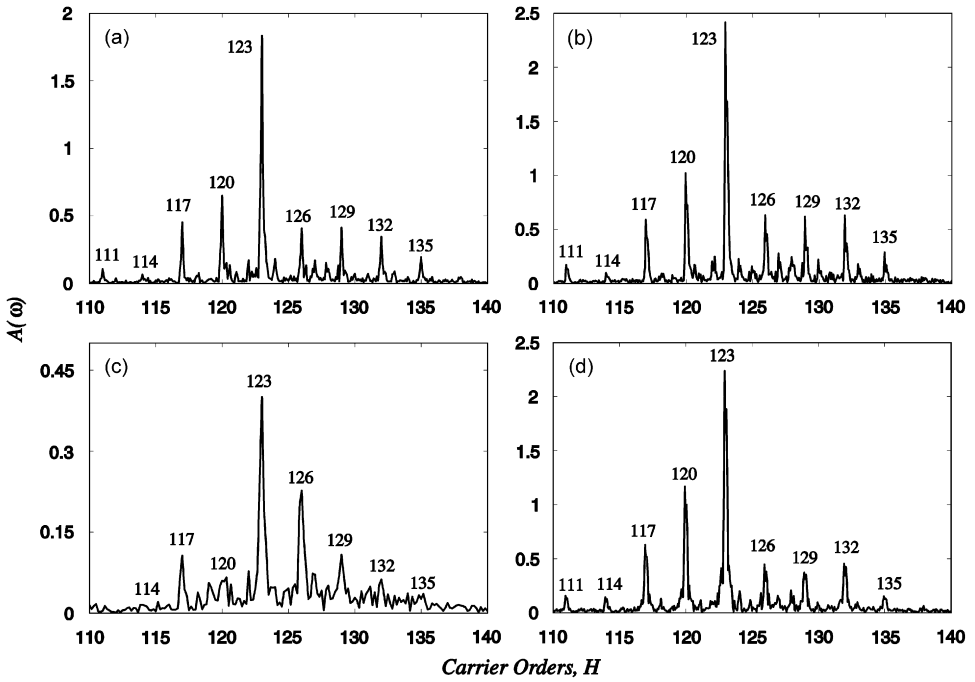

Fig. 13. Examples of measured $A(\omega)$ order spectra for the gear set A at different torque and speed conditions: (a) $T_s = 500$ Nm, $\Omega_s = 400$ rev/min, (b) $T_s = 600$ Nm, $\Omega_s = 500$ rev/min, (c) $T_s = 200$ Nm, $\Omega_s = 200$ rev/min, and (d) $T_s = 1000$ Nm, $\Omega_s = 500$ rev/min.

Fig. 13 shows order spectra from gear set A (Case (ii) type with equally spaced and sequentially phased planets) at various T_s and Ω_s values, focusing on the activity around H_m. The first major observation from these spectra is that no harmonic order is apparent at $H_m = 125$, i.e. $A_m \approx 0$. All significant harmonic orders with sizable amplitudes are at orders $H = nN = \ldots, 117, 120, 123, 126, 129, 132, \ldots$ in the vicinity of mesh harmonic order H_m. Sidebands are not symmetric about H_m. All these observations agree with the predicted spectra of Fig. 4(a) and the sideband behavior established in Section. 2 for Case (ii) gear sets. One difference is that predicted harmonic order with the largest amplitude was the order $H = nN = 126$ that is closest to

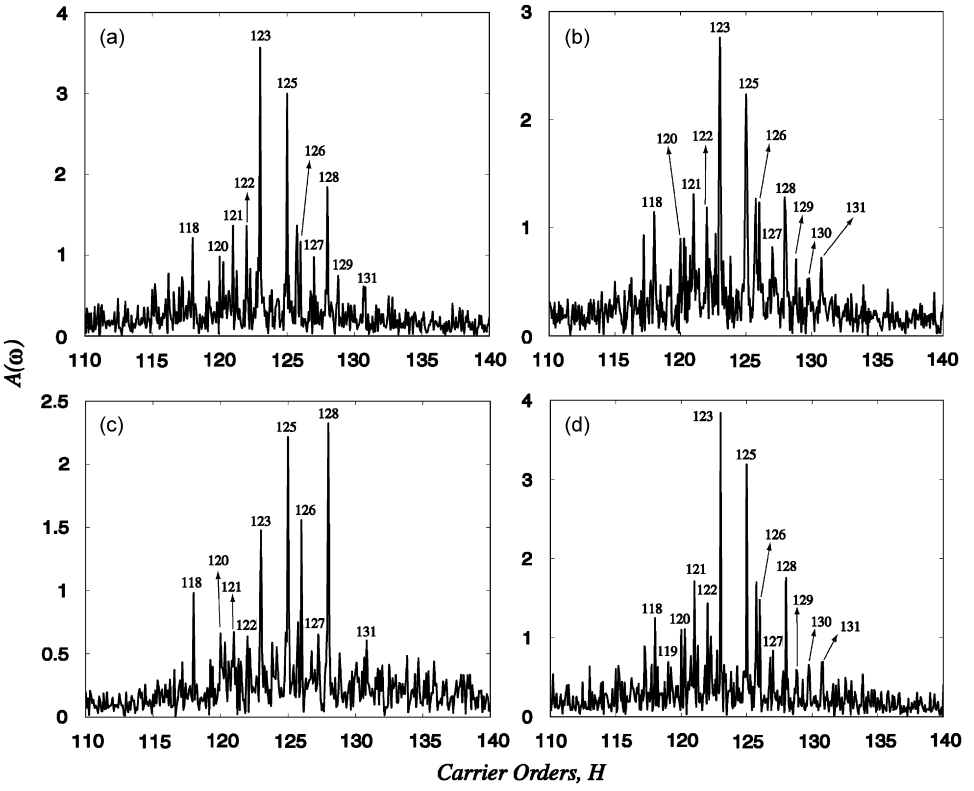

Fig. 14. Examples of measured $A(\omega)$ order spectra for the gear set B at different torque and speed conditions: (a) $T_s = 400$ Nm, $\Omega_s = 500$ rev/min, (b) $T_s = 500$ Nm, $\Omega_s = 500$ rev/min, (c) $T_s = 800$ Nm, $\Omega_s = 400$ rev/min, and (d) $T_s = 1000$ Nm, $\Omega_s = 500$ rev/min.

$H_m = 125$ while $A_{\max}$ is observed at $H = 123$ in the measured spectra shown in Fig. 13. It is also noted that relative amplitudes of the sideband orders vary with T_s and Ω_s due to dynamic effects that were not included in this model.

Similarly, Fig. 14 shows the spectra from gear set B at four different T_s and Ω_s combinations. For this Case (iv) type gear set (unequally spaced and sequentially phased), the measured sideband activity carries the most of the common features drawn from the analytical study. Specifically, sideband harmonics appear at several integer multiples of the carrier order at $H_m \pm n$ (n: integer) in an asymmetric way around H_m. The number of sidebands with tangible amplitudes is rather high (10–15). In addition, as both Z_r and N are odd numbers, the gear mesh harmonic order $H_m = 125$, while non-zero, does not represent the largest amplitude.

Finally in Fig. 15, four measured $A(\omega)$ spectra are shown for gear set C (Case (v) type with unequally spaced and arbitrarily phased planets). In line with Fig. 7(b), these measured spectra exhibit a rich sideband activity with sideband orders at $H_m \pm n$ that are asymmetric about H_m. The gear mesh harmonic order has small amplitudes as in predictions of Fig. 7(b). Only main difference between these measurements and the predictions from the simplified model is that experiments provide a full sideband spectrum with components at $H_m \pm n$ while the predicted spectrum for this X-shaped 4-planet gear set (N: even) reveals more dominant even sideband orders. This suggests that there might be other mechanisms that are not included in the simplified analysis such as FM and unequal planet load sharing characteristics.

It is consistently observed in Figs. 13–15 that the most dominant harmonic order with the maximum amplitude is $H = 123$ while the model predicts the order $H = 126$ (order that is closest to $H_m = 125$) as the dominant one. The factors that were not included in the proposed simplified model such as unequal planet load sharing, ring gear deflections as well as manufacturing errors of gears (especially roundness error of the ring gear) could be a reason for this discrepancy. Our ongoing modeling effort attempts to include these factors through more detailed discrete and deformable-body dynamic models.

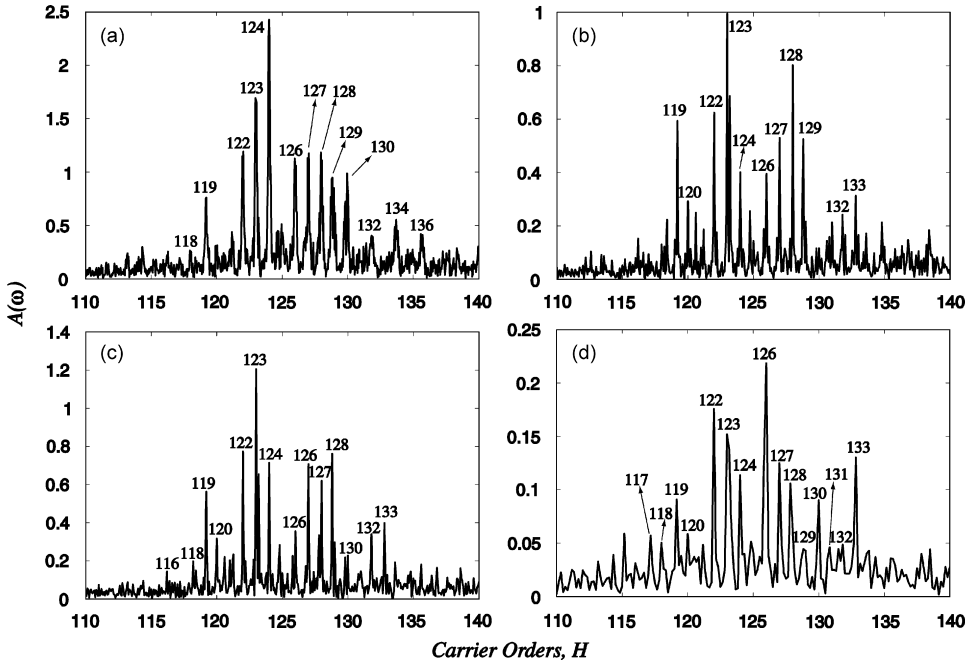

Fig. 15. Examples of measured $A(\omega)$ order spectra for the gear set C at different torque and speed conditions: (a) $T_s = 200$ Nm, $\Omega_s = 800$ rev/min, (b) $T_s = 400$ Nm, $\Omega_s = 500$ rev/min, (c) $T_s = 600$ Nm, $\Omega_s = 500$ rev/min, and (d) $T_s = 1000$ Nm, $\Omega_s = 200$ rev/min.

4. Conclusions and future work

In this study, modulation sidebands of planetary gear sets were investigated analytically and experimentally. First, a simplified analytical model was proposed to predict the modulation sideband orders as well as relative amplitude distributions in the vicinity of the mesh frequency harmonic orders. The model considered the number of planets, planet position angles and the number of teeth of the stationary gear (sun or ring) as the sole parameters defining the resultant sideband activity. The model was used to simulate a wide range of gear sets to show that any planetary gear set can be classified in one of five distinct groups: (i) equally spaced and in-phase planets, (ii) equally spaced and sequentially phased planets, (iii) unequally spaced and in-phase planets, (iv) unequally spaced and sequentially phased planets, and (v) unequally spaced and arbitrarily phased planets. General sideband behavior unique to each of these cases were characterized and demonstrated through simulation of various gear sets. Based on this behavior, other general conclusions can be made as follows:

(1) In a sequentially phased planetary gear set, sidebands are always asymmetrically distributed about the mesh orders.
(2) A dominant (and maximum) mesh harmonic amplitude is achieved only when the planet meshes are in phase ($Z_r/N =$ integer).
(3) Symmetric sidebands in both frequencies and amplitudes about the mesh frequency are possible only when the gear set is in-phase and equally spaced.

A special-purpose experimental set-up was developed to check the validity of the conclusions of the model. The experimental study included gear sets from three of the five distinct cases identified by the model. Comparison of the measured spectra to the predictions and general behavior presented in Section 2 indicated that the model, while simple in many aspects, is capable of capturing the bulk of the sideband behavior. Measurements also revealed qualitatively different behavior for the three gear sets considered in support of the classification of planetary gear set arrived at based on this model. With this, the general trends unique to each

of the five cases of gear sets can be deemed valid, as they were observed in the experimental data as well. They also point to other influences caused by the dynamic effects at different speeds as well as the changes in gear mesh excitations with the torque transmitted. Accordingly, our current work focuses incorporating this analytical model with a discrete parameter, nonlinear time-varying dynamic model similar to the one proposed by Kahraman [24] to predict the gear mesh dynamic forces and sidebands associated with manufacturing errors specified in Section 1. An experimental and analytical study is also underway to investigate sideband behavior of gear sets having unequal planet load sharing. Finally, a finite elements based deformable-body model of a planetary gear set is being developed for prediction of sideband amplitudes quantitatively for various ring gear rim thickness values.

Acknowledgments

Authors would like to thank Dr. A. Singh of General Motors Powertrain for allowing the use of the test fixtures and gear specimens in this study.

References

[1] H. Ligata, A. Kahraman, A. Singh, An experimental study on the influence of manufacturing errors on the planetary gear stresses and planet load sharing, *ASME Journal of Mechanical Design* 130 (2008) 041701-1–041701-9.
[2] A. Bodas, A. Kahraman, Influence of carrier and gear manufacturing errors on the static load sharing behavior of planetary gear sets, *JSME International Journal—Series C* 47 (3) (2004) 908–915.
[3] A. Kahraman, G.W. Blankenship, Planet mesh phasing in epicyclic gear sets, *Proceedings of International Gearing Conference*, Newcastle UK, September 1994, pp. 99–104.
[4] A. Kahraman, Planetary gear train dynamics, *ASME Journal of Mechanical Design* 116 (1994) 713–720.
[5] G.W. Blankenship, R. Singh, Analytical solution for modulation sidebands associated with a class of mechanical oscillators, *Journal of Sound and Vibration* 179 (1) (1995) 13–36.
[6] L. Bellomonte, I. Guastella, R.M. Sperandeo-Mineo, Mechanical models of amplitude and frequency modulation, *European Journal of Physics* 26 (2005) 409–422.
[7] T. Hidaka, Y. Terauchi, K. Ishioka, Dynamic behavior of planetary gear (2nd report: displacement of sun gear and ring gear), *Bulletin of the JSME* 19-138 (1976) 1563–1570.
[8] P.D. McFadden, J.D. Smith, An explanation for the asymmetry of the modulation sidebands about the tooth meshing frequency in epicyclic gear vibration, Proceedings of the Institution of Mechanical Engineers 199 (C1) (1985) 65–70.
[9] P.D. McFadden, A technique for calculating the time domain averages of the vibration of the individual planet gears and the sun gear in an epicyclic gearbox, *Journal of Sound and Vibration* 144 (1) (1991) 163–172.
[10] J. McNames, Fourier series analysis of epicyclic gearbox vibration, *ASME Journal of Vibration and Acoustics* 124 (2002) 150–152.
[11] C.E. Fair, Synchronous sampling sideband orders from helical planetary gear sets, MS Thesis, Virginia Polytechnic Institute and State University, 1998.
[12] A.L. Gu, R.H. Badgley, T. Chiang, Planet-pass-induced vibration in planetary reduction gears, *ASME Design Engineering Technical Conference*, Paper No. 74-DET-93, New York, NY, USA, October 1974.
[13] A.L. Gu, R.H. Badgley, Prediction of vibration sidebands in gear meshes, *ASME Design Engineering Technical Conference*, Paper No. 74-DET-95, New York, NY, USA, October 1974.
[14] P.P. Schon, Unconditionally Convergent Time Domain Adaptive and Time-frequency Techniques for Epicyclic Gearbox Vibration, ME Thesis, The University of Pretoria, June 2005.
[15] A.M. Mitchell, F.B. Oswald, H.H. Coe, Testing of UH-60A helicopter transmission in NASA Lewis 2240 kW (3000 hp) Facility, NASA Technical Paper 2626, August 1986.
[16] M. Mosher, Results from a new separation algorithm for planetary gear system vibration measurements, *Proceedings of ASME International Design Engineering Technical Conferences and Computers and Information in Engineering Conference*, Paper No. DETC-84404, California, USA, September 2005.
[17] M. Mosher, Understanding vibration spectra of planetary gear systems for fault detection, *Proceedings of ASME Design Engineering Technical Conferences*, Paper No. PTG-48082, IL, USA, September 2003.
[18] D.G. Lewicki, J.J. Coy, Vibration characteristics of OH-58A helicopter main rotor transmission, NASA Technical Paper 2705, 1987.
[19] A. Saxena, B. Wu, G. Vachtsevanos, A methodology for analyzing vibration data from planetary gear systems using complex morlet wavelets, *2005 American Control Conference*, Portland, OR, USA, June 2005, pp. 4730–4735.
[20] D.M. Blunt, J.A. Keller, Detection of a fatigue crack in a UH-60A planet gear carrier using vibration analysis, *Mechanical Systems and Signal Processing* 20 (2006) 2095–2111.
[21] R. Patrick-Aldaco, A Model Based Framework for Fault Diagnosis and Prognosis of Dynamical Systems with an Application to Helicopter Transmissions, PhD Thesis, Georgia Institute of Technology, August 2007.

[22] J.A. Hines, D.S. Muench, J.A. Keller, A.K. Garga, Effects of time-synchronous averaging implementations on HUMS features for UH-60A planetary carrier cracking, *American Helicopter Society 61st Annual Forum*, Paper No: VA 22314–2538, Grapevine, TX, USA, June 2005.
[23] J.A. Keller, P. Grabill, Vibration monitoring of UH-60A main transmission planetary carrier fault, *American Helicopter Society 59th Annual Forum*, Phoenix, AZ, USA, May 2003.
[24] A. Kahraman, Load sharing characteristics of planetary transmissions, *Mechanism and Machine Theory* 29 (8) (1994) 1151–1165.
[25] M. Inalpolat, A. Kahraman, Dynamic modelling of planetary gears of automatic transmissions, Proceedings of the Institution of Mechanical Engineers Part K: Journal of Multi-body Dynamics 222 (2008) 229–242.
[26] A. Al-shyyab, A. Kahraman, A non-linear dynamic model for planetary gear sets, *Proceedings of the Institution of Mechanical Engineers Part K: Journal of Multi-Body Dynamics* 221 (2007) 567–576.
[27] A. Singh, A. Kahraman, H. Ligata, Internal gear strains and load sharing in planetary transmissions—model and experiments, *ASME Journal of Mechanical Design* 130 (2008) 072602-1–072602-10.
[28] H. Ligata, Impact of System-level Factors on Planetary Gear Set Behavior, PhD Thesis, The Ohio State University, 2007.